Pergamon

Acta mater. Vol. 46, No. 17, pp. 6245–6256, 1998
© 1998 Acta Metallurgica Inc.
Published by Elsevier Science Ltd. All rights reserved
Printed in Great Britain
1359-6454/98 $19.00 + 0.00

PII: S1359-6454(98)00254-7

ROOM-TEMPERATURE MECHANICAL BEHAVIOR OF FeAl: EFFECTS OF STOICHIOMETRY, ENVIRONMENT, AND BORON ADDITION

J. W. COHRON[1,2], Y. LIN[1,2], R. H. ZEE[2] and E. P. GEORGE[1]†

[1]Metals and Ceramics Division, Oak Ridge National Laboratory, Oak Ridge, TN 37831-6093, U.S.A. and [2]Materials Engineering Program, Auburn University, Auburn, AL 36849-5351, U.S.A.

(Received 9 June 1998; accepted 3 July 1998)

Abstract—The intrinsic ductility of FeAl (in ultrahigh vacuum) decreases with increasing Al content, from around 16% in Fe–37Al to zero in Fe–48Al. The sharpest decline occurs around the composition where the fracture mode changes from transgranular to intergranular. Boron shifts this ductile–brittle transition to higher Al levels by segregating to the grain boundaries and suppressing grain-boundary fracture. However, its effectiveness decreases with increasing Al concentration, even though the amount of B segregating to the grain boundaries remains the same, independent of alloy stoichiometry. Consequently, even the B-doped alloys become brittle and fracture intergranularly as the stoichiometric composition is approached. Low-pressure hydrogen embrittles FeAl, although not as severely as atmospheric moisture. Environmental embrittlement is most noticeable in Fe-rich FeAl; with increasing Al concentration, the grain boundaries become intrinsically weak, and brittle fracture persists even after environmental effects are eliminated.
© 1998 Acta Metallurgica Inc. Published by Elsevier Science Ltd. All rights reserved.

1. INTRODUCTION

The B2 structure of FeAl is stable over a wide composition range: from approximately Fe–36Al (compositions in at.%, unless noted otherwise) to approximately the stoichiometric composition (Fe–50Al) at temperatures around 400°C [1]. Deviations from stoichiometry are thus restricted almost entirely to the Fe-rich side (at low temperatures) and are accommodated by Fe anti-site atoms [2, 3]. Triple defects—two vacancies on the Fe sublattice in combination with an Fe anti-site atom on the Al sublattice—are also present, especially near the stoichiometric composition [4–6]. At room temperature, plastic deformation in FeAl occurs by the movement of antiphase-boundary-coupled $a/2\langle 111\rangle$ dislocations on the $\{110\}$ planes [7, 8].

FeAl alloys have long been known to be brittle in air. Their brittleness persists over the entire range of B2-phase stability, with practically no tensile ductility in the near-stoichiometric alloys and only 2–3% elongation even in the Fe-rich ones [9–12]. The fracture mode of FeAl in air depends sensitively on stoichiometry: those alloys that contain less than about 40% Al fail by transgranular cleavage [9, 11, 13, 14], whereas those that contain more Al fail by grain-boundary fracture [9, 13–15]. The exact composition at which this transition between transgranular and intergranular fracture occurs depends on factors such as grain size, point defect concentration, grain boundary impurities, etc. For example, Fe–40Al samples that have not been given a long-term, low-temperature anneal to eliminate vacancies fail predominantly by intergranular fracture [15, 16], whereas those alloys given the long-term anneal exhibit more transgranular fracture [14].

Moisture-induced environmental embrittlement [11, 15–18] has been shown to be a leading cause of brittleness in Fe-rich FeAl. When its effects are reduced (by testing in vacuum or under cover gases such as O_2), FeAl (36.5Al) can be quite ductile, with elongations to fracture as high as 18% in dry oxygen [15]. Atomic hydrogen, generated by a reaction between the Al atoms in FeAl and water vapor in air, was suggested as the chemical species responsible for this embrittlement [11]. X-ray photoelectron spectroscopy coupled with temperature-programmed desorption from water-vapor-exposed surfaces of monocrystalline $Ni_3(Al,Ti)$ [19] and polycrystalline TiAl, FeAl and NiAl alloys [20] has confirmed that Al is the element responsible for the dissociation of water.

Environmental embrittlement is not the only reason for poor ductility and brittle fracture in FeAl alloys. With increasing Al concentration, another factor, namely intrinsic grain-boundary weakness, becomes important in limiting the ductility of FeAl [16]. At intermediate compositions (e.g. Fe–40Al), both environmental embrittlement and poor grain-boundary cohesion limit the ductility of FeAl, and both have to be overcome to get good ductility [16].

†To whom all correspondence should be addressed.

Small additions of B, on the order of a few hundred wppm, are known to improve the ductility of some ordered intermetallics (e.g. Refs [10, 21–24]). In the case of FeAl, boron has been shown to segregate to the grain boundaries [15, 16] and suppress intergranular fracture [9, 10, 15, 16]. However, by itself, it is not able to significantly improve ductility [15, 16]. The reason is that environmental embrittlement occurs transgranularly in FeAl [16], unlike, say, in Ni_3Al, where it occurs intergranularly [25–27]. Consequently, grain-boundary segregation of B can suppress environmental embrittlement in Ni_3Al [25, 26], but not in FeAl where it occurs transgranularly [16]. The beneficial role of B in FeAl appears to be related mainly to the enhancement of grain-boundary cohesion.

In the present study, we investigate the "intrinsic" mechanical behavior of FeAl (i.e. in the absence of extrinsic environmental effects), and determine the effects of alloy stoichiometry and B doping. We also investigate the effects of dry H_2 on the ductilities of FeAl alloys and compare its effects with those of moisture and oxygen. In order to eliminate any effects that quenched-in vacancies may have on mechanical properties, all the alloys in this study were given a five-day anneal at 673 K to minimize the thermal vacancy concentrations [28].

2. EXPERIMENTAL PROCEDURE

2.1. Alloy preparation

Four binary FeAl alloys, containing 37, 40, 45, and 48% Al, were produced by arc melting followed by drop casting into cylindrical copper molds. For comparison, four B-doped alloys containing 300 wppm B and 40, 43, 45 and 48% Al were also arc melted and drop cast. An Fe–4 wt.% B master alloy was used for the boron doping. There was negligible weight loss (typically $<0.5\%$) during the melting and casting, indicating that the actual alloy compositions were close to the aim compositions. The cast ingots, having approximate dimensions of 127 mm (height) and 25 mm (diameter), were canned in mild steel billets and hot-extruded at a 9:1 ratio. The extrusion temperatures for each alloy are given in Table 1.

2.2. Tensile tests in air and oxygen

Buttonhead specimens (gage diameter, 1.84 mm; gage length, 12.25 mm) were fabricated from the extruded ingots of B-doped Fe–43Al, Fe–45Al and Fe–48Al alloys with their long axes parallel to the extrusion direction. The specimens were first electropolished to reduce surface defects and then given the following heat treatment in vacuum ($\sim 7 \times 10^{-4}$ Pa): 1 h at 1173 K + 2 h at 973 K + 5 days at 673 K. The first two steps were for recrystallization (which established the grain size) and B2 ordering, respectively, whereas the purpose of the last step was to anneal out the thermal vacancies generated at the higher temperatures of the first two steps. Room-temperature tensile tests were performed in air and oxygen on an Instron machine equipped with a vacuum chamber. For the oxygen tests, the chamber was first evacuated to $\sim 7 \times 10^{-4}$ Pa and purged with oxygen several times. Oxygen was then leaked into the chamber through a Varian leak valve until its pressure (monitored with a Granville–Phillips Convectron gage) reached $\sim 6.7 \times 10^{4}$ Pa. Both the air and oxygen tests were conducted at room temperature at a strain rate of 3.3×10^{-3}/s. Ductility was obtained by dividing the change in total specimen length by the initial gage length (all the elongation was assumed to occur in the gage section).

2.3. Tensile tests in UHV and hydrogen

Dog-bone specimens with two different gage sections were utilized for these tensile tests. The first set of specimens, with gage sections measuring $3.2 \times 1.6 \times 0.5$ (mm), were electro-discharge machined (EDM) from the extruded ingots of B-doped Fe–40Al and B-free Fe–45Al with their long axes parallel to the extrusion direction. Each specimen then had ~0.08 mm removed from their EDM surfaces by grinding prior to annealing in vacuum ($\sim 7 \times 10^{-4}$ Pa) for 1 h at either 1158 K (B-doped Fe–40Al) or 1203 K (B-free Fe–45Al), followed by 5 days at 673 K for both alloys. As before, the first temperature established the grain size while the long-term anneal served to minimize thermal vacancies. After annealing, all the specimens were hand polished to reduce surface defects, finishing

Table 1. Extrusion temperatures, heat treatments and grain sizes of alloys investigated in this study

Alloy	Extrusion temperature (K)	Heat treatment	Grain size (μm)
Fe–37Al	1173	1073 K/1 h + 673 K/5 days	85
Fe–40Al	1223	1073 K/1 h + 673 K/5 days	80
Fe–45Al	1173	1203 K/1 h + 673 K/5 days	110
Fe–48Al	1173	1073 K/1 h + 673 K/5 days	60
Fe–40Al + 300 wppm B	1173	1158 K/1 h + 673 K/5 days	55
Fe–40Al + 300 wppm B	1173	1073 K/1 h + 673 K/5 days	25
Fe–43Al + 300 wppm B	1073	1173 K/1 h + 973 K/2 h + 673 K/5 days	25
Fe–45Al + 300 wppm B	1073	1173 K/1 h + 973 K/2 h + 673 K/5 days	118
Fe–45Al + 300 wppm B	1073	1073 K/1 h + 673 K/5 days	22
Fe–48Al + 300 wppm B	1073	1173 K/1 h + 973 K/2 h + 673 K/5 days	25
Fe–48Al + 300 wppm B	1073	1073 K/1 h + 673 K/5 days	15

with 4000 grit SiC paper. Another set of specimens, having a somewhat larger gage section of $7.4 \times 1.7 \times 0.5$ (mm), were EDM from the remaining alloys (i.e. B-free Fe–37Al, Fe–40Al, Fe–48Al; and B-doped Fe–40Al, Fe–45Al, Fe–48Al). These specimens were also polished to remove surface defects. For convenience, all the specimens in the second set were given the same grain-size anneal of 1073 K for 1 h followed by a vacancy-removal anneal at 673 K for 5 days. This resulted in some variation in the grain sizes of these specimens; however, as discussed later in this paper, it did not significantly affect ductility. Alloy compositions, extrusion temperatures, annealing temperatures/times, and the resulting grain sizes are summarized in Table 1.

Room-temperature tensile testing was performed in an ultrahigh vacuum (UHV) chamber equipped with two liquid-nitrogen-cooled sorption pumps and an ion pump. The base pressure in the chamber after bake-out, and prior to tensile testing, was usually less than $\sim 1 \times 10^{-7}$ Pa. A hydrogen bottle (99.9999%, research purity) was connected by copper tubing (part of which was coiled and immersed in a liquid nitrogen cold trap to eliminate all traces of moisture) to a Varian leak valve attached to the UHV chamber. Dry H_2 was then leaked into the UHV chamber until the desired pressure was reached. Additional details of the experimental setup have been described previously [29].

Because of the smaller gage sections of the specimens used in the UHV and hydrogen tests, their lengths were measured using an optical microscope equipped with a translation stage. Fiducial marks were inscribed at the ends of the radii on all the specimens tested. Ductility was obtained by measuring the change in length between the fiducial marks divided by the initial length. Because of the two different gage lengths of these specimens, the strain rate was either 5×10^{-4} or 1.2×10^{-3}/s. This variation is not expected to affect our results because these strain rates are both in the range where the room-temperature ductility of FeAl is relatively insensitive to strain rate [30, 31].

2.4. Auger and scanning electron microscopy

The fracture surfaces of the tensile specimens were examined in a scanning electron microscope to determine their fracture modes. A PHI 590 scanning Auger microprobe was utilized to study the segregation of B to the grain boundaries. Notched specimens were machined from the gage sections of tensile-tested specimens and loaded into the UHV of the Auger microprobe. They were fractured *in situ* by striking with a sharp hammer blow. The Auger analyses were carried out in the pulse counting mode with a 5 kV primary electron beam and beam currents of ~8 nA. Approximately 25 grain boundaries were analyzed in each specimen. The 703 eV iron and 1398 eV aluminum peaks were used to calculate their grain-boundary concentrations relative to their bulk concentrations (i.e. the average composition of the transgranular areas was employed as a standard). Unfortunately, the same could not be done for B (since the amount of B in the bulk was below the detectable limit); therefore, the 179 eV boron peak was used in conjunction with the Fe and Al peaks and their respective elemental sensitivity factors [32] to calculate the B concentration at the grain boundaries. This introduces some uncertainty in the absolute values of the calculated B concentrations; however, the relative values from one specimen to the next are expected to be reliable because the same procedure was used in each case.

3. RESULTS

3.1. Boron-free FeAl

Figure 1 shows the room-temperature ductility in UHV of B-free FeAl as a function of Al concentration. For comparison, data from earlier work [12, 16], which were obtained in vacuum (10^{-4} Pa), air, and O_2 are also included. At all the compositions, specimens tested in air are the most brittle, followed by those tested in vacuum, oxygen, and UHV. Ductility drops off sharply with increasing Al concentration until there is no observable plasticity when the Al level reaches 48%. At the lower Al concentrations, the O_2 data and the UHV data compare well but, at the higher Al levels, ductilities are higher in UHV than in O_2. The two sets of air data differ somewhat, for reasons that are outlined in the Discussion section.

The fracture surfaces of the B-free FeAl alloys tested in UHV are shown in Fig. 2. As the aluminum concentration increases, the fracture mode changes from transgranular to intergranular. The fracture mode was approximately 100% transgranular for the Fe–37Al alloy and nearly 100% intergranular for the Fe–48Al alloy. At intermediate compositions (Fe–40Al and Fe–45Al) the alloys exhibited a mixed mode of fracture (Table 2).

Figure 3 shows the elongation to fracture of B-free FeAl as a function of hydrogen pressure. The most comprehensive data are for the alloy containing 37% Al which show that, as the hydrogen pressure increases, the ductility decreases from ~16% in UHV to ~9% at 1300 Pa. The 40 and 45% Al alloys had relatively low ductilities in UHV (~5%), which appeared to remain constant as the hydrogen pressure increased. The Fe–48Al alloy showed no tensile elongation, even in UHV. In general, ductility was independent of whether the ion gage (a device used to measure gas pressures whose hot tungsten filament is known to dissociate molecular H_2 into atomic H) was on or off. This contrasts with our earlier observation that the ductility of B-free Ni_3Al remains high in molecular H_2 (when the ion gage is off), but drops sharply (by as

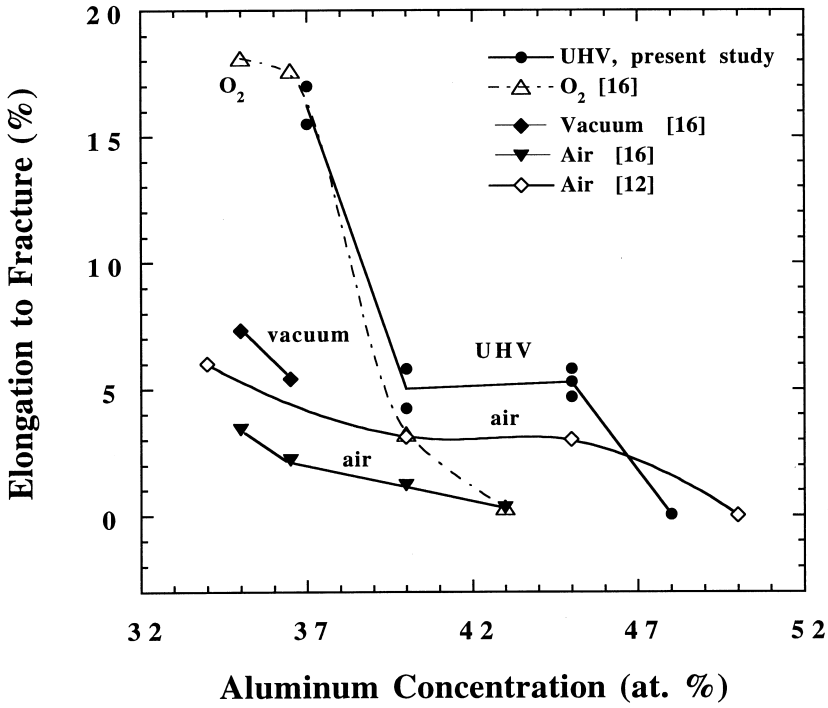

Fig. 1. Elongation to fracture of B-free FeAl alloys in different environments as a function of Al concentration.

much as a factor of four) in atomic H (when the ion gage is turned on) [29]. The fracture modes in H_2 were similar to those in UHV (i.e. fracture became increasingly intergranular with increasing Al concentration) and showed no change with increasing hydrogen pressure at a given Al level.

3.2. Boron-doped FeAl

Figure 4 shows the room-temperature ductility in air, O_2, and UHV, of B-doped FeAl as a function of Al concentration. For comparison, data from earlier work [33] obtained in vacuum ($\sim 10^{-4}$ Pa) are also included. The elongation to fracture in UHV was the highest, followed by that in O_2, vacuum, and air. In all the environments tested, ductility decreases with increasing Al concentration. Along with the ductility measurements, at the top of Fig. 4, grain-boundary B concentrations (measured by Auger electron spectroscopy, see below) are presented as a function of Al content. Note that the B level at the grain boundaries is independent of the Al concentration in the bulk.

The fracture surfaces of the B-doped FeAl alloys tested in UHV are shown in Fig. 5. As the Al concentration increases, the fracture mode changes from transgranular to intergranular. Similar behavior was observed also in air and O_2; in other words, the fracture mode depended only on the Al concentration and not the test environment. Broadly similar behavior was noted also in B-free FeAl (Fig. 2). However, unlike in B-free FeAl, in B-doped FeAl, small regions of transgranular cleavage ($< 5\%$ of the total fracture surface area) could be observed even in the 48% Al alloy. It is not clear if this difference was due to the smaller grain size of the B-doped alloy (Table 1). Regardless, the important point to note in Fig. 5 is that the ability of B to suppress intergranular fracture decreases as the Al concentration approaches the stoichiometric composition, despite the fact that it segregates just as strongly as in the Fe-rich alloys (Fig. 4).

Figure 6 shows the elongation to fracture of B-doped FeAl as a function of H_2 pressure. The most comprehensive data are for the 40 and 45% alloys and show that, as the H_2 pressure increases, ductility decreases. In UHV, the B-doped Fe–40Al alloy had the highest elongation to fracture, ~17%, which decreased to ~8% at 6.7×10^3 Pa. For the Fe–45Al alloy, the ductility in UHV was ~12%, which fell to ~8% at 1.3×10^3 Pa. The Fe–48Al alloy had a relatively low ductility (~5%) in UHV, which remained unchanged as the H_2 pressure was increased.

Auger analysis was used to study the grain-boundary chemistry of the 43, 45, and 48% Al alloys. Figure 7 shows a typical Auger spectrum obtained from a grain boundary in the Fe–43Al alloy. Besides the Fe, Al and B peaks, small C and O peaks also appear in the spectrum. Since similar C and O peaks were present also in the transgranular regions, it is assumed that they were the result of contamination after fracture in the Auger system.

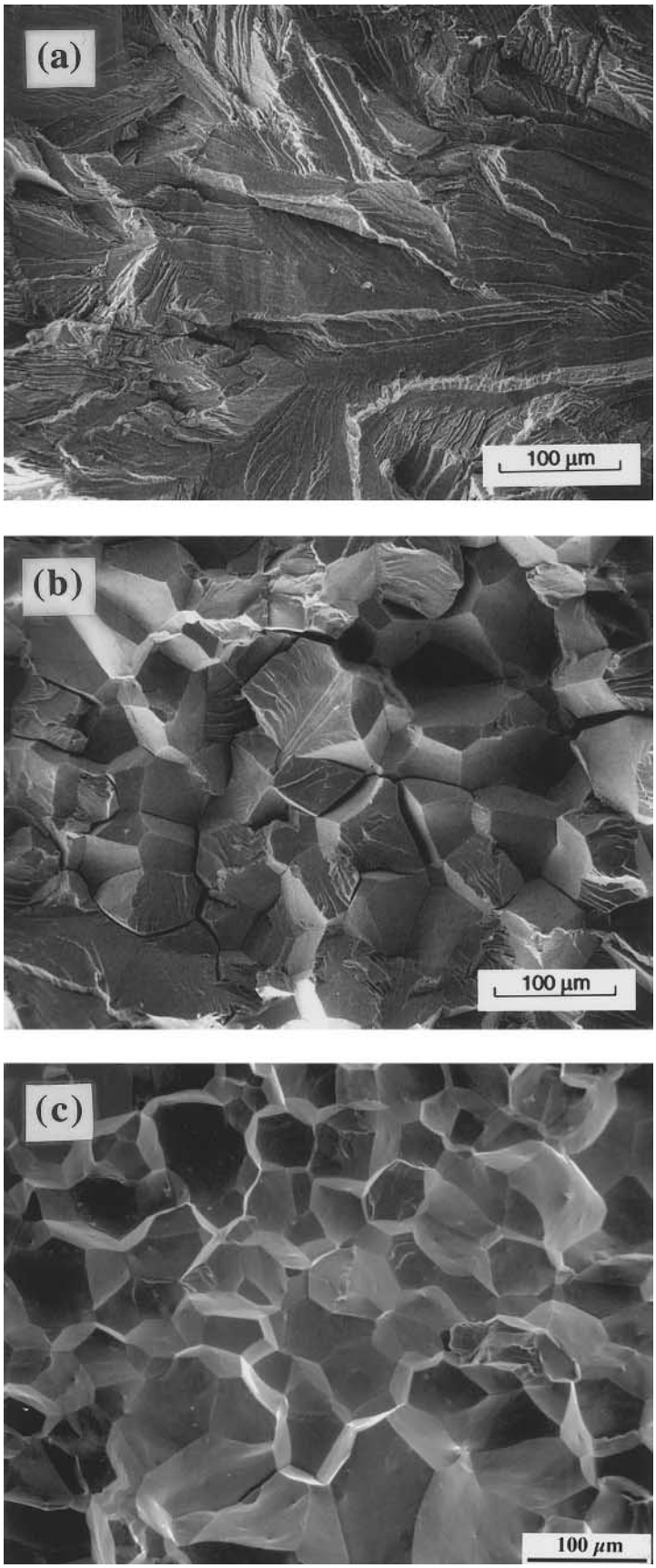

Fig. 2. Typical fracture surfaces of B-free FeAl alloys: (a) Fe–37Al, (b) Fe–45Al and (c) Fe–48Al. Note the change from transgranular to intergranular fracture with increasing Al concentration.

Table 2. Fracture modes of B-free and B-doped FeAl alloys investigated in this study

Alloy	Fracture mode	
	O_2	UHV
Fe–37Al	Transgranular	Transgranular
Fe–40Al	—	Mixed
Fe–43Al	—	—
Fe–45Al	—	Mixed
Fe–48Al	—	Intergranular
Fe–40Al + 300 wppm B	Transgranular (traces of IG†)	Transgranular (traces of IG)
Fe–43Al + 300 wppm B	Mostly transgranular	—
Fe–45Al + 300 wppm B	Mixed	Mixed
Fe–48Al + 300 wppm B	Intergranular	Intergranular (traces of TG‡)

† Intergranular.‡ Transgranular.

A boron peak was clearly visible on the grain boundaries of all three alloys. Table 3 lists the average B levels, atomic concentrations of Al at the grain boundaries, and the peak height ratios (Al/Fe) for transgranular and intergranular regions in the three alloys. The average B concentrations are 4.3% in Fe–43Al, 4.3% in Fe–45Al, and 4.9% in Fe–48Al. The average atomic concentrations of Al in the grain boundaries were calculated from the Al/Fe peak height ratios and the results indicate that there is no significant depletion of Al at the boundaries in these three alloys (relative to the bulk).

4. DISCUSSION

This is the first study to investigate the effects of stoichiometry on the ductility and fracture behavior of FeAl in the virtual absence of environmental effects (i.e. in UHV). Our results are summarized in Fig. 8. In UHV, the ductility of well-annealed B-free FeAl drops off precipitously as the aluminum concentration increases beyond 37% Al. Since tests conducted in UHV presumably measure the "intrinsic" ductility, the present results show that FeAl becomes intrinsically brittle when its composition approaches the stoichiometric composition. Additionally, the fracture mode changes from transgranular to intergranular as the ductility decreases. Together, these results confirm an earlier suggestion [16], which was based on tests conducted in oxygen, that the grain boundaries in FeAl become intrinsically brittle as the Al concentration increases.

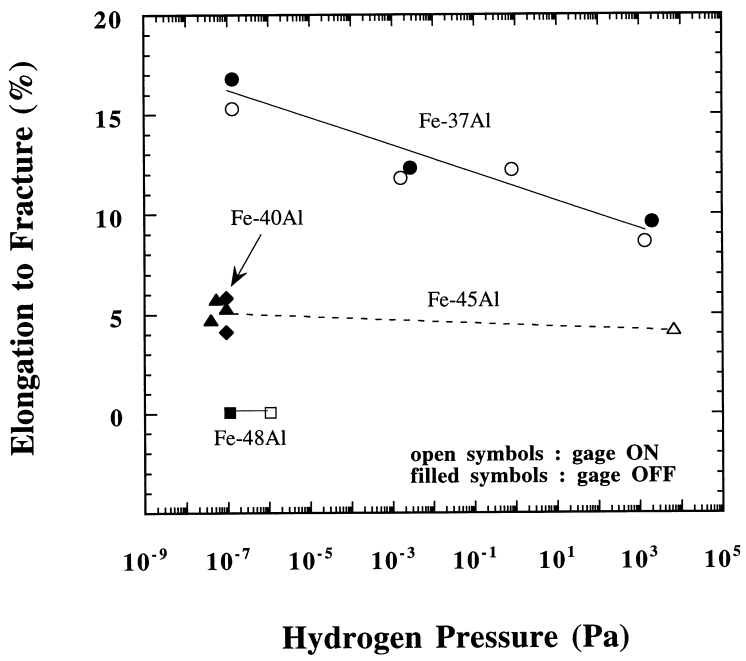

Fig. 3. Elongation to fracture of B-free FeAl alloys as a function of hydrogen pressure.

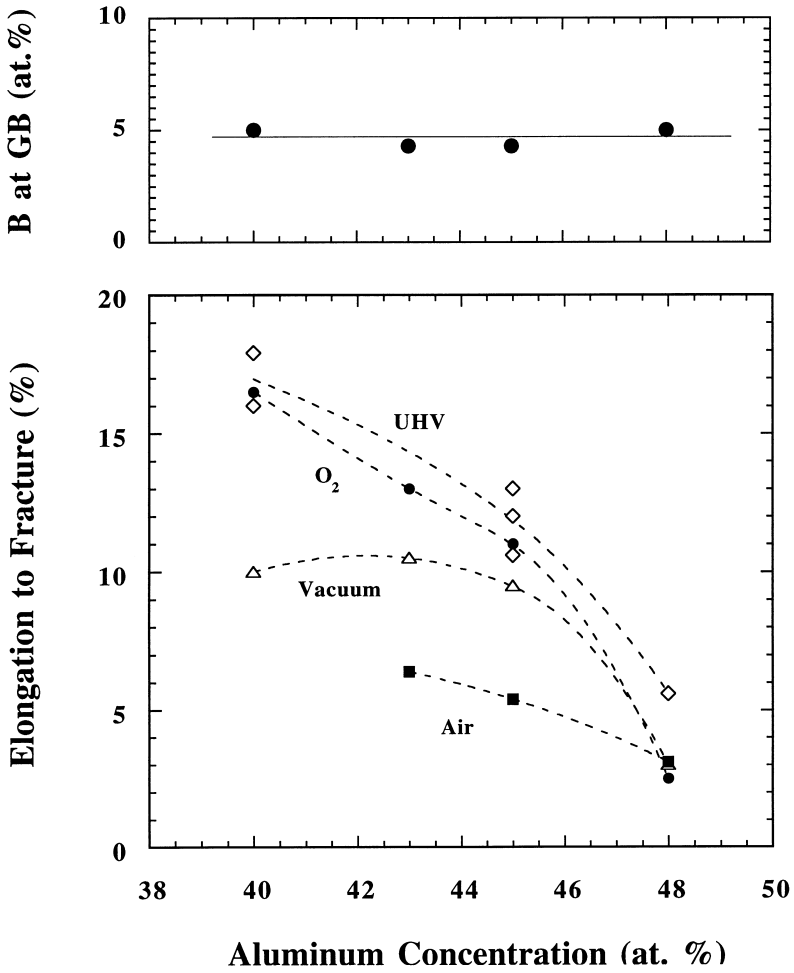

Fig. 4. Elongation to fracture of B-doped FeAl alloys in different environments as a function of Al concentration (vacuum data from Ref. [33], and O_2 data for Fe–40Al from Ref. [15]). Also included (at top) are the average grain-boundary concentrations of B as a function of Al concentration (Fe–40Al data from Ref. [15]).

When B is added to FeAl, intergranular fracture is suppressed and the composition at which the ductility drops off is shifted to higher Al levels (Fig. 8). As shown previously in one alloy (Fe–40Al [15]), and confirmed in this study over a range of stoichiometries (Fig. 4), the beneficial effect of B stems from its segregation to the grain boundaries where it presumably enhances grain-boundary cohesion. However, with increasing Al concentration, B is less able to suppress intergranular fracture in FeAl (Fig. 8). A similar behavior was noted also in Ni_3Al [24]. In that case, however, B segregated less strongly to the grain boundaries of Ni_3Al as the Al concentration increased [24]. In the present study, by contrast, the segregation of B is essentially independent of Al concentration (Fig. 4). Apparently, the grain boundaries in near-stoichiometric FeAl become so weak that, even though B segregates strongly, it is unable to strengthen them. Another difference between Ni_3Al and FeAl is that, in the former, the main role of B is to suppress moisture-induced embrittlement at the grain boundaries [25, 26], whereas in the latter, its main role is to enhance grain-boundary cohesion. (Grain-boundary B has little effect on environmental embrittlement in FeAl because it occurs transgranularly.)

In general, the B-doped alloys have finer grain sizes than the B-free alloys (Table 1). Therefore, it is fair to ask whether the grain-size difference between the two sets of alloys is the main reason for the change in ductility and fracture mode discussed above, rather than any effect of B *per se*. To answer this, we tested two different grain sizes of B-doped Fe–45Al (22 and 118 μm, Table 1). These values are at the extremes of the grain-size range tested in this study. Three specimens with a grain size of 22 μm were tested in UHV and had ductilities of 10.6, 12.0 and 13% whereas a specimen with a grain size of 118 μm was tested in O_2 and had a comparable ductility of 10.7%. Furthermore, the B-doped Fe–45Al alloys have similar ductilities in

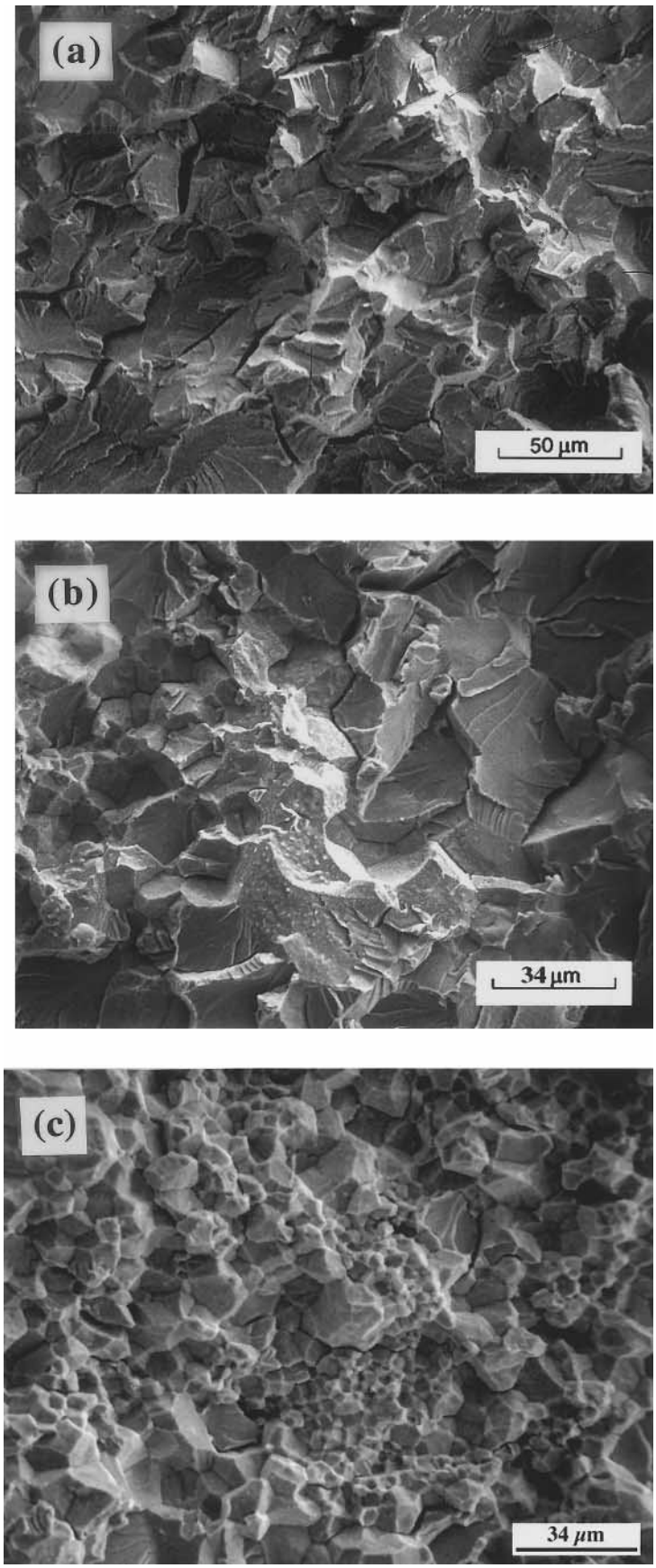

Fig. 5. Typical fracture surfaces of B-doped FeAl alloys: (a) Fe–40Al, (b) Fe–45Al, and (c) Fe–48Al.

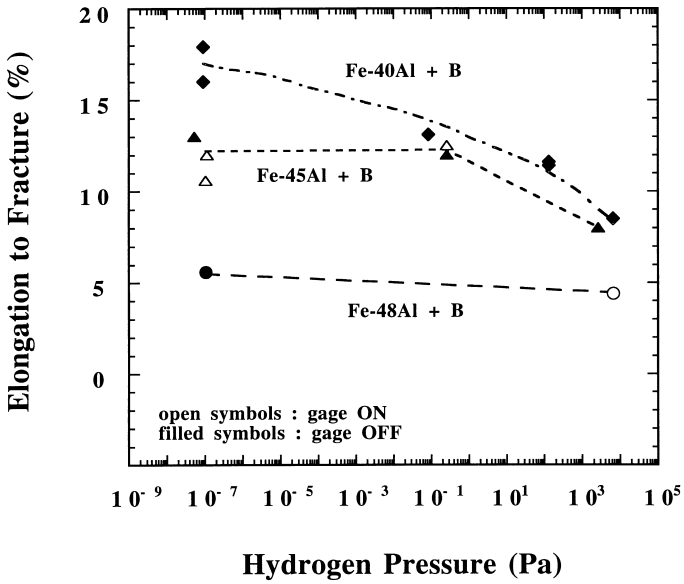

Fig. 6. Elongation to fracture of B-doped FeAl alloys as a function of hydrogen pressure.

UHV and vacuum (Fig. 4)—which are significantly higher than the ductility of B-free Fe–45Al (Fig. 1)—despite the fact that one of the B-doped alloys has a much larger grain size (comparable to that of the B-free alloy). Clearly, boron has a beneficial effect of its own, beyond any indirect effect it may have through grain refinement. That said, there is some evidence to suggest that grain refinement may improve the ductility of FeAl (to a limited extent). As shown in Fig. 1, the ductilities obtained by Nagpal and Baker [12] (in alloys with grain sizes of ~20 μm) are higher than those obtained by Liu and George [16] (in alloys with grain sizes of ~150 μm). Unfortunately, this interpretation is confounded by the fact that Nagpal and Baker gave their alloys a long-term vacancy-removal anneal, whereas Liu and George did not. Therefore, the higher ductilities obtained by Nagpal and Baker may be only partly due to their finer grain size (part of the difference may be due to their lower vacancy concentrations).

When environmental embrittlement is the main cause of brittle fracture, tests in oxygen yield the same ductility as those in UHV (e.g. the Fe-rich alloys in Fig. 1). This result differs from that obtained in Ni_3Al [27, 29], where the ductility in UHV was found to be significantly higher than that in oxygen. In general, considerably less residual water vapor is expected in a baked-out UHV chamber than in an unbaked turbo-pumped chamber back-filled with O_2 [27]. Therefore, FeAl appears to be less sensitive to environmental embrittlement than Ni_3Al. Also, FeAl is not as intrinsically ductile as Ni_3Al, because its highest ductility in UHV (~16% for Fe–37Al, Fig. 1) is considerably lower than that of Ni_3Al in UHV (~40% in Ni–23.4Al, [29]).

The environmental influences on ductility dwindle as the Al concentration increases until, at Al levels approaching the stoichiometric composition, the intrinsic ductility of FeAl is so low that brittle fracture persists even after environmental effects are virtually eliminated (by testing in UHV). In other words, as the Al concentration in FeAl increases, environmental embrittlement becomes one of two factors, rather than the single factor limiting ductility (as is the case at lower Al concentrations).

One of the objectives of this study was to compare the embrittling effect of dry H_2 with that of moisture in air. In previous work [11, 15] it was shown that atmospheric moisture severely embrittles Fe–36.5Al: its ductility decreased from ~18% in dry oxygen to ~2% in air [15]. Compared to this, the ductility decrease in dry H_2 is much more modest: as shown in Fig. 3, the elongation to fracture of Fe–37Al decreases from ~16% in UHV to only about 9% in 1300 Pa hydrogen. This H_2 pressure (1300 Pa) is comparable to the partial pressure of water vapor in atmospheric air (assuming 50% relative humidity) [27]. Therefore, at similar pressures, dry H_2 does not embrittle FeAl as severely as does water vapor. A similar observation was noted also in Ni_3Al [29]. In fact, molecular H_2 hardly embrittles Ni_3Al at all [29], unlike in FeAl, where some H_2-induced embrittlement is evident (Fig. 3). Another difference is that, in FeAl, the ion gage had no discernible effect on ductility (Fig. 3), unlike in Ni_3Al where ductility dropped by as much as a factor of four when the ion gage was turned on [29]. We conclude, therefore, that the dissociation of

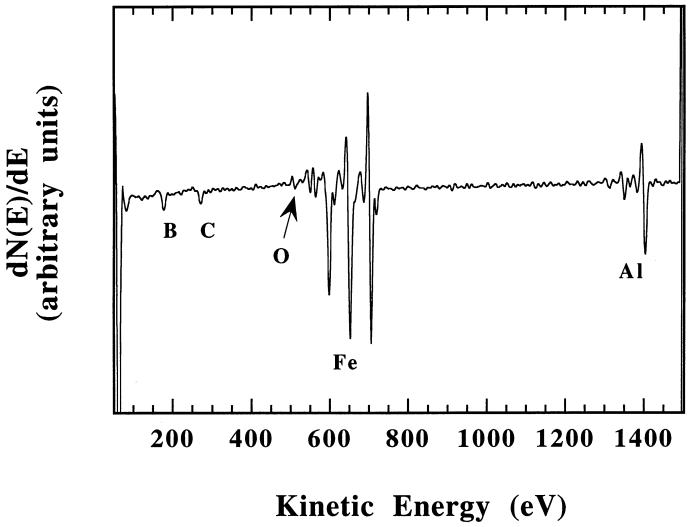

Fig. 7. Typical Auger spectrum from a grain boundary of B-doped Fe–43Al. The small C and O peaks are a result of post-fracture contamination in UHV.

molecular H_2 into atomic H is more efficient on the fracture surfaces of FeAl than on Ni_3Al.

The embrittling effect of H_2 on B-doped FeAl (Fig. 6) is almost identical to its effect on B-free FeAl (Fig. 3), with one main difference: the environmental effect is discernible at higher Al concentrations in the B-doped alloys as compared to the B-free alloys. This difference may be rationalized as follows. In the absence of B, the grain boundaries in alloys containing >40% Al constitute the weakest links during fracture. As a result, brittle intergranular fracture occurs in these alloys, independent of the H_2 pressure (i.e., these alloys are so brittle that any additional embrittling effect of H_2 is difficult to detect). When B is added, it strengthens the grain boundaries. As a result, the embrittling effect of H_2 is discernible at somewhat higher Al levels.

5. CONCLUSIONS

The intrinsic ductility (measured in UHV) of B-free FeAl decreases with increasing Al concentration, from ~16% in Fe–37Al to zero in Fe–48Al. The sharpest decline occurs between 37 and 40% Al where the fracture mode changes from transgranular to intergranular.

Boron shifts this ductile–brittle transition to higher Al levels by segregating to the grain boundaries and suppressing grain-boundary fracture.

The ability of B to suppress grain-boundary fracture decreases with increasing Al concentration, although the amount segregating to the grain boundaries remains the same, independent of alloy stoichiometry. Consequently, even the B-doped alloys become brittle and fracture intergranularly as the stoichiometric composition is approached.

Low-pressure H_2 embrittles otherwise ductile FeAl: the ductilities of B-free Fe–37Al and B-doped Fe–40Al (and to a lesser extent B-doped Fe–45Al) decrease with increasing H_2 pressure. At higher Al concentrations, intrinsic grain-boundary weakness is the dominant factor limiting ductility; therefore, H_2-induced embrittlement becomes harder to detect (i.e. the alloys remain brittle even after environmental effects are eliminated).

Table 3. Summary of AES results for FeAl alloys investigated in this study

Alloy	Auger PHR† (Al/Fe) IG‡	Auger PHR† (Al/Fe) TG§	GB¶ Al (at.%)	Auger PHR (B/Fe) IG	GB B (at.%)
Fe–43Al + 300 wppm B	0.38 ± 0.02	0.38 ± 0.03	42.9	0.05 ± 0.02	4.3 ± 1.4
Fe–45Al + 300 wppm B	0.42 ± 0.02	0.41 ± 0.02	45.6	0.06 ± 0.02	4.3 ± 1.4
Fe–48Al + 300 wppm B	0.47 ± 0.05	0.46 ± 0.04	48.0	0.07 ± 0.03	5.0 ± 2.0

† Peak high ratio.‡ Intergranular.§ Transgranular.¶ Grain boundary.

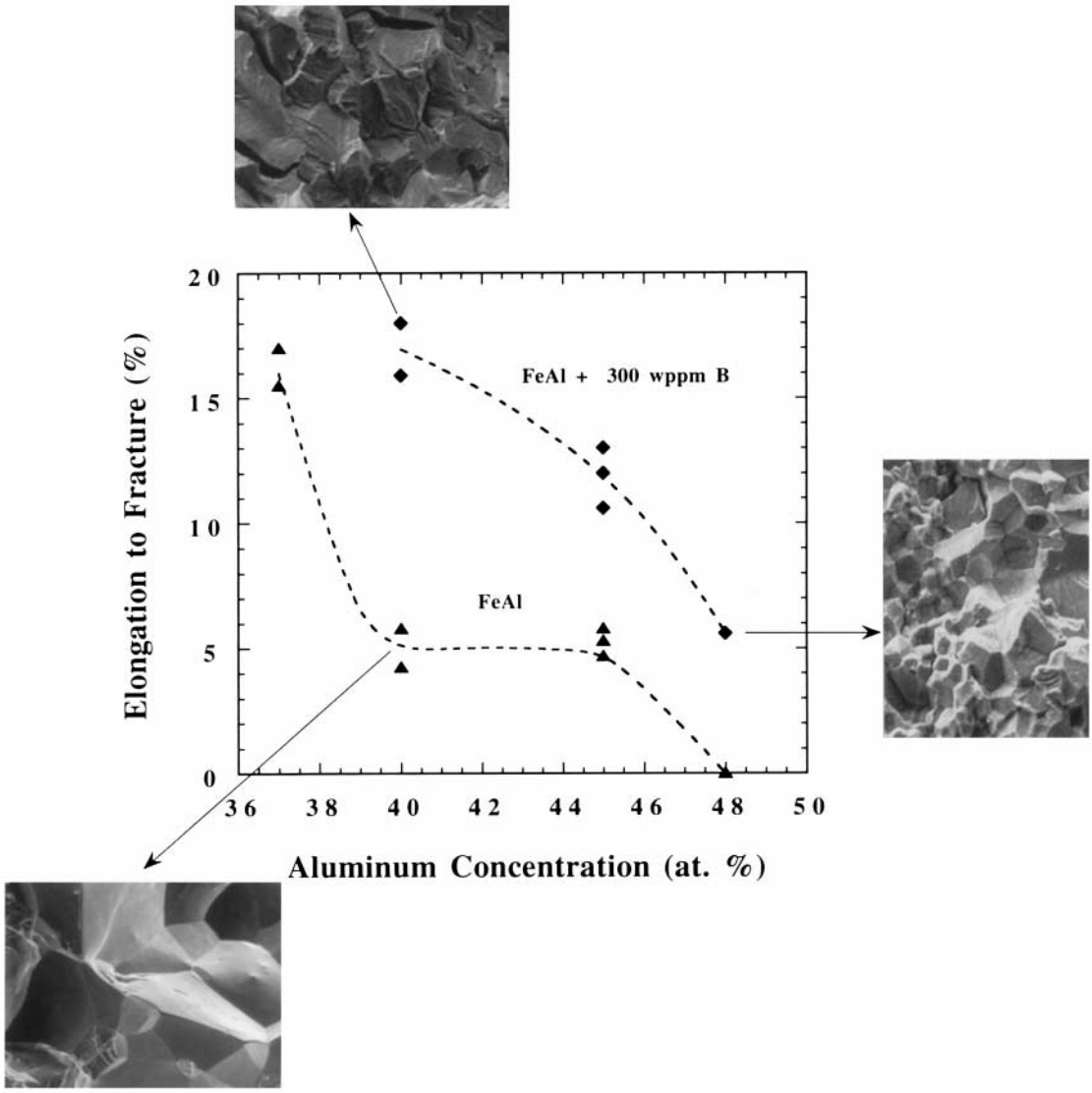

Fig. 8. Comparison of the effects of alloy stoichiometry and B doping on the ductility and fracture mode of FeAl alloys in UHV.

Atmospheric moisture is more detrimental than molecular H_2 to the ductilities of both B-free and B-doped FeAl alloys.

Acknowledgements—This research was sponsored by the Division of Materials Sciences, U.S. Department of Energy under contract DE-AC05-96OR22464 with Lockheed Martin Energy Research Corp.

REFERENCES

1. Massalski, T. B. (ed.), *Binary Alloys Phase Diagrams*, Vol 1. ASM International, Materials Park, OH, 1986, p. 112.
2. Wertheim, G. K. and Wernick, J. H., *Acta metall.*, 1967, **15**, 297.
3. Huffman, G. P. and Fisher, R. M., *J. appl. Phys.*, 1967, **38**, 735.
4. Wasilewski, R. J., *J. Phys. Chem. Solids*, 1968, **29**, 39.
5. Neumann, J. P., Chang, Y. A. and Lee, C. M., *Acta. metall.*, 1976, **24**, 593.
6. Riviere, J. P., *Mater. Res. Bull.*, 1977, **12**, 995.
7. Umakoshi, Y. and Yamaguchi, M., *Phil. Mag. A*, 1980, **41**, 573.
8. Munroe, P. R. and Baker, I., *Acta metall. mater.*, 1991, **39**, 1011.
9. Crimp, M. A. and Vedula, K. M., *Mater. Sci. Engng*, 1986, **78**, 193.
10. Crimp, M. A., Vedula, K. M. and Gaydosh, D. J., *Mater. Res. Soc. Symp. Proc.*, 1987, **81**, 499.
11. Liu, C. T., Lee, E. H. and McKamey, C. G., *Scripta metall.*, 1989, **23**, 875.
12. Nagpal, P. and Baker, I., *Mater. Char.*, 1991, **27**, 167.
13. Gaydosh, D. J. and Crimp, M. A., *Mat. Res. Soc. Symp. Proc.*, 1985, **39**, 429.
14. Baker, I. and Gaydosh, D. J., *Mater. Sci. Engng*, 1987, **96**, 147.
15. Liu, C. T. and George, E. P., *Scripta metall. mater.*, 1990, **24**, 1285.

16. Liu, C. T. and George, E. P., *Mater. Res. Soc. Symp. Proc.*, 1991, **213**, 527.
17. Liu, C. T., Fu, C. L., George, E. P. and Painter, G. S., *Iron Steel Inst. Japan International*, 1991, **31**, 1192.
18. Gaydosh, D. J. and Nathal, M. V., *Scripta metall. mater.*, 1990, **24**, 1281.
19. Chia, W. J. and Chung, Y. W., *Intermetallics*, 1995, **3**, 505.
20. Gleason, N. R., Gerken, C. A. and Strongin, D. R., *Appl. Surf. Sci.*, 1993, **72**, 215.
21. Aoki, K. and Izumi, O., *J. Japan. Inst. Metals*, 1979, **43**, 1190.
22. Aoki, K., *Mater. Trans. Japan. Inst. Metals*, 1990, **31**, 443.
23. Liu, C. T., *Scripta metall.*, 1991, **25**, 1231.
24. Liu, C. T., White, C. L. and Horton, J. A., *Acta metall.*, 1985, **33**, 213.
25. Cohron, J. W., George, E. P., Heatherly, L., Liu, C. T. and Zee, R. H., *Acta mater.*, 1997, **45**, 2801.
26. George, E. P., Liu, C. T. and Pope, D. P., *Acta mater.*, 1996, **44**, 1757.
27. George, E. P., Liu, C. T. and Pope, D. P., *Scripta metall. mater.*, 1994, **30**, 37.
28. Nagpal, P. and Baker, I., *Metall. Trans.*, 1990, **21A**, 2281.
29. Cohron, J. W., George, E. P., Heatherly, L., Liu, C. T. and Zee, R. H., *Intermetallics*, 1996, **4**, 497.
30. Baker, I., Klein, O., Nelson, C. and George, E. P., *Scripta metall. mater.*, 1994, **30**, 863.
31. Nagpal, P. and Baker, I., *Scripta metall. mater.*, 1991, **25**, 2577.
32. Davis, L. E., MacDonald, N. C., Palmberg, P. W., Riach, G. E. and Weber, R. E., *Handbook of Auger Electron Spectroscopy*. Physical Electronics Industries, Inc., Eden Prairie, MN, 1976.
33. Carleton, R., George, E. P. and Zee, R. H., *Intermetallics*, 1995, **3**, 433.